Hindawi
Advances in Materials Science and Engineering
Volume 2018, Article ID 9290306, 8 pages
https://doi.org/10.1155/2018/9290306

Research Article

Optical-Fiber-Based Smart Concrete Thermal Integrity Profiling: An Example of Concrete Shaft

Ruoyu Zhong, Ruichang Guo, and Wen Deng

Missouri University of Science and Technology, Rolla, MO, USA

Correspondence should be addressed to Wen Deng; wendeng@mst.edu

Received 5 April 2018; Accepted 29 July 2018; Published 9 September 2018

Academic Editor: Andrey E. Miroshnichenko

Concrete is currently the most widely used construction material in the world. The integrity of concrete during the pouring process could greatly affect its engineering performance. Taking advantage of heat production during the concrete curing process, we propose an optical-fiber-based thermal integrity profiling (TIP) method which can provide a comprehensive and accurate evaluation of the integrity of concrete immediately after its pouring. In this paper, we use concrete shaft as an example to conduct TIP by using the optical fiber as a temperature sensor which can obtain high spatial resolution temperature data. Our method is compared with current thermal infrared probe or embedded thermal sensor-based TIP for the concrete shaft. This innovation makes it possible to detect defects inside of the concrete shaft with thorough details, including size and location. First, we establish a 3D shaft model to simulate temperature distribution of concrete shaft. Then, we extract temperature distribution data at the location where the optical fiber would be installed. Based on the temperature distribution data, we reconstruct a 3D model of the concrete shaft. Evaluation of the concrete integrity and the existence of the potential defect are shown in the paper. Overall, the optical-fiber-based TIP method shows a better determination of defect location and size.

1. Introduction

Concrete is currently the most widely used construction material all over the world. Concrete consists of both fine and coarse aggregates that are bonded by cement paste. Hydration reaction occurs when cement is blended with water. This hydration is an exothermal reaction, which means it generate heat and results in temperature rise during concrete curing. At the beginning, tricalcium aluminate (C_3A) reacts with water and generates a large amount of heat, but the reaction would not last long. It is followed with a short period that release less heat called the dormant phase. After a short period of dormancy, the alite and belite start to react and continuously generate heat. The maximum heat generation would last 10 to 20 hours after pouring. Since cementitious material can generate a large amount of heat, defects of concrete would lead to temperature divergence in the concrete structure. By taking advantage of such a feature of concrete, we propose an innovative method of optical fiber-based thermal integrity profiling (TIP) to inspect the concrete integrity and use the concrete shaft as an example to demonstrate the method.

Since the concrete shaft serves as the deep foundation, the quality of the concrete shaft is critical for the safety of superstructures. Defects within the concrete shaft would degrade the shaft performance (Figure 1). The existence of defects within the concrete shaft is mainly due to some problems of construction and design deficiencies [1]. Among 5,000 to 10,000 shafts tested, 15% of shafts showed the deviation from ideal signal and 5% of tested shafts showed indisputable defect indication [2, 3]. Since both excavation and concreting are blind processes when building drilled shafts, it is impossible to completely prevent defects from happening during construction. Determination of whether defects exist in the concrete shaft and how severe the defects are, are crucial to evaluate whether the concrete shaft would satisfy its design purpose. Among the existing methods, nondestructive testing is a widely accepted method for shaft integrity testing.

Currently, major nondestructive testing methods include low strain integrity test and cross-hole sonic logging (CSL). The low strain integrity test, also known as sonic pulse echo method, uses light hammer impacts and evaluates the

(a) (b) (c) (d)

Figure 1: Different kinds of defects (images are from an online source).

collected force and velocity recordings to evaluate shaft integrity [4–6]. The low strain integrity test is cost-efficient and effective. However, this method has limitations including operator's familiarity and experience, and length/width ratio of the concrete shaft. CSL is a widely used nondestructive integrity test method. For CSL, 3–8 access tubes must be installed within a shaft cross section [7]. Then, a signal generator coupled with receiver is lowered, maintaining a consistent elevation, to test the integrity of concrete shaft. This method has higher accuracy, but is limited within the reinforcement cage. The CSL method only tests the integrity of concrete shaft between the access tubes, while outside of that zone is left untested. However, the bending capacity of the concrete shaft is mainly dependent on the outer part. The core of the concrete shaft has little contribution to bending capacity [8, 9]. The integrity of the outer part of concrete shaft should be evaluated as well.

TIP, which is a new nondestructive testing method, makes use of the hydration heat generated during concrete curing to determine whether defects exist and estimates their size and location according to the temperature distribution along the concrete shaft [10–12]. Temperature distribution is measured by lowering a thermal probe with infrared thermocouples into access tubes or by an embedded thermal sensor during the curing process. Inverse modeling of temperature distribution would provide information on whether the reinforcement cage has been misplaced or improper formation has happened. In addition, the location and type of defect would be indicated from the data. A relatively cool region indicates a shortage of concrete at that particular location, whereas a relatively warm region indicates extra concrete. Compared with previous methods, TIP covers a larger area and provides a more comprehensive result. However, due to the limited amount of access tubes, temperature data for inverse modeling could be insufficient to accurately predict temperature distribution of the concrete shaft which could limit further development of this method [11, 13].

Referring to advancements in optical fiber studies, Rayleigh scattering caused by local refractive index fluctuations along the glass fiber can be used to measure strains and temperature. Every point on the optical fiber can send a different Rayleigh scattering signal when subjected to temperature change, and therefore, every point along the fiber acts as a temperature sensor [14–18]. This feature of optical fibers makes it an ideal temperature sensor to measure high spatial resolution temperature distribution. Currently, this technology has been applied to measuring and recording temperature data, for example, in car engines, microwave ovens, or large furnaces for the steel industry. Advances in the research on Rayleigh scattering-based optical fiber make its application on TIP possible. By applying this optical fiber to TIP as a temperature sensor, more comprehensive and consistent temperature data can be provided. The conventional method sets an access tube every 300 mm diameter, and a measurement point within access tubes with vertical intervals less than 500 mm. In this optical-fiber based method, the optical fiber would be wrapped around the reinforcement cage spirally and densely with negligible cost of the fiber itself. Even if the vertical interval is the same as the conventional method when wrapping the optical fiber, the horizontal interval would still be significantly smaller. Temperature data measured by optical-fiber-based TIP would have high spatial resolution. The measured temperature data interval can be as small as 4 mm. Thus, the inverse modeling of temperature distribution can produce a more reliable integrity report [19–22].

The objective of this paper is to address the advantages of our proposed optical-fiber-based TIP method regarding its inverse modeling of temperature distribution of defected concrete shaft by having high resolution spatial temperature data. We used finite element method (FEM) to simulate temperature distribution of a defective concrete shaft. Temperature data were extracted in two different ways based on the concepts of our new method and conventional infrared thermal probe method. Based on the temperature distribution data, we reconstructed the 3D geometry of concrete shaft based on two methods. The impact of the size and location of the defect on temperature distribution is discussed in this paper.

2. Methodology

2.1. Governing Equation. The principle of TIP is to take advantage of the correlation between the shape of the concrete shaft and temperature distribution. The temperature distribution is simulated using FEM. The governing equation of temperature (T) distribution in concrete shaft is as follows:

$$\frac{\rho C_p \partial T}{\partial t} = \left[\frac{\partial}{\partial x}\left(k\frac{\partial T}{\partial x}\right) + \frac{\partial}{\partial y}\left(k\frac{\partial T}{\partial y}\right) + \frac{\partial}{\partial z}\left(k\frac{\partial T}{\partial z}\right)\right] + Q, \tag{1}$$

where C_p represents the heat capacity of the material, k is the thermal conductivity of the material, and Q is the heat source of the material.

2.2. Heat Generation. The total amount of heat production and the rate of heat production are two important factors of temperature distribution. These two factors determine the temperature of the concrete shaft and the timing for TIP to be performed. The amount of heat and heat production rate are related to the ingredients of the concrete. Concrete with different proportions would generate different amounts of heat. The total heat production can be determined by using the following equations [23]:

$$\begin{aligned} Q_0 &= Q_{\text{cem}} p_{\text{cem}} + 461 p_{\text{slag}} + Q_{\text{FA}} p_{\text{FA}}, \\ Q_{\text{cem}} &= 500 p_{C_3S} + 260 p_{C_2S} + 866 P_{C_3A} + 420 p_{c_4AF} \\ &\quad + 624 p_{SO_3} + 1186 p_{\text{FreeCaO}} + 850 p_{\text{MgO}}, \\ Q_{\text{FA}} &= 1800 p_{\text{FACaO}}. \end{aligned} \tag{2}$$

The degree of hydration can be determined by the following equations [10, 23]:

$$\begin{aligned} \alpha(t) &= \alpha_u \exp\left(-\left[\frac{\tau}{t_e}\right]^{\beta}\right), \\ \alpha_u &= \frac{(1.031 w/\text{cm})}{(0.194 + w/\text{cm})} + 0.5 p_{\text{FA}} + 0.3 p_{\text{SLAG}} < 1, \\ \beta &= p_{C_3S}^{0.227} \cdot 181.4 \cdot p_{C_3A}^{0.146} \cdot \text{Blaine}^{-0.535} \cdot p_{SO_3}^{0.558} \\ &\quad \cdot \exp\left(-0.647 p_{\text{SLAG}}\right), \\ \tau &= p_{C_3S}^{-0.401} \cdot 66.78 \cdot p_{C_3A}^{-0.154} \cdot \text{Blaine}^{-0.804} \cdot p_{SO_3}^{-0.758} \\ &\quad \cdot \exp\left(2.187 \cdot p_{\text{SLAG}} + 9.5 \cdot p_{\text{FA}} \cdot p_{\text{FACaO}}\right), \end{aligned} \tag{3}$$

where $\alpha(t)$ represents the degree of hydration of cement at time t, w/cm is the water-cement ratio, and β and τ are determined by the cementitious constituent fractions. According to ASTM D7949-14, the recommended timing to perform TIP would be 12 hours after concrete placement until the number of days is equivalent to the foundation diameter in meters divided by 0.3 m.

2.3. Heat Transport. Heat transport is another important factor for temperature evolution within the concrete shaft. Heat is dissipated into the surrounding soil simultaneously after heat is generated due to hydration. Heat transport includes three mechanisms: conduction, convection, and radiation. In this situation, heat conduction is the predominant mechanism in heat transport. Heat conduction in the material is represented by thermal conductivity k.

Soil consists of solids, air, and water. The specific value of thermal conductivity of soil is determined by the constitution of soil and the thermal conductivity of each phase. The thermal conductivity can be determined by using the following equation [24–26]:

$$k_1 = k_s - n[k_s - S_w k_w - (1 - S_w)k_a], \tag{4}$$

where n denotes porosity and S_w represents the degree of saturation.

However, this model does not consider the effect caused by the shape of the void inside of soil. Thus, they introduce a shape factor $\chi = \sqrt{S_w}$ into the equation to represent the effect caused by the shape of the void. Then, the equation becomes

$$k = \sqrt{S_w}\{k_s - n[k_s - S_w k_w - (1 - S_w)k_a]\} + (1 - \sqrt{S_w})k_a. \tag{5}$$

2.4. Heat Capacity. We assume that the temperature of the soil is the same among the three phases and that the heat capacity of the soil is also related to the three phases. The heat required to raise the temperature of soil one degree can be calculated by $C_s m_s + C_w m_w + C_g m_g$. The total weight of the soil is $m_s + m_w + m_g$. Therefore, the value of soil heat capacity can be determined as follows:

$$C_p = \frac{C_s m_s + C_w m_w + C_g m_g}{m_s + m_w + m_g}. \tag{6}$$

Considering that the mass of air is negligible, the equation can be simplified as

$$C_p = \frac{C_s + C_w w}{1 + w}, \tag{7}$$

where w is water content.

2.5. Simulation Parameters. A common concrete shaft consists of two parts: concrete and reinforcement cage. To get the data of temperature distribution, the sensor must be deployed inside of concrete shaft. As mentioned above, the optical fiber would be wrapped around the reinforcement cage spirally so that temperature along the fiber would be obtained. When it comes to conventional TIP, temperature can only be measure through access tubes or at the points where embedded sensors are set.

In order to simulate the temperature evolution and distribution within the shaft, a 3D model is established as shown in Figure 2. The model consists of four parts: concrete inside reinforcement cage, concrete outside reinforcement cage, soil surrounding shaft, and soil below shaft. In this

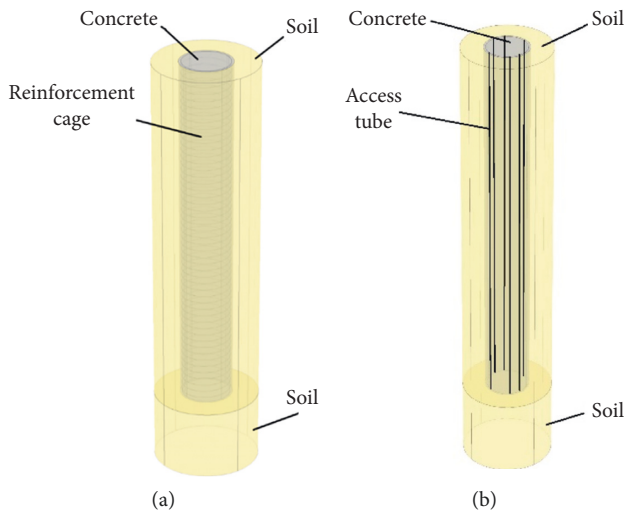

Figure 2: Shaft-soil model.

case, heat transfer into the reinforcement cage has been neglected since the reinforcement cage has a low heat capacity, high thermal conductivity, and relatively small volume. However, simulation of the reinforcement cage surface is still necessary because the reinforcement cage is where the optical sensor and access tubes are deployed. The location of the reinforcement cage surface would be the interface between the core concrete cylinder and the concrete cover. To get as much data as possible for high spatial resolution temperature distribution data, optical fiber is chosen to be deployed spirally. The pitch of optical fiber is 300 mm. To simulate access tubes in the conventional TIP method, we use vertical lines to represent the access tubes. According to ASTM D7949-14, one access duct should be placed every 300 mm in diameter. Therefore, there would be 6 vertical lines on the reinforcement cage in our setting.

The thickness of soil outside the concrete shaft is chosen based on the distance between two concrete shafts. In this case, the thickness is equal to the diameter of the concrete shaft. The properties of soil are listed in Table 1.

This simulation was conducted using FEM. The mesh type is free tetrahedral, with the minimum element size of 0.21 m. Several defects would be set on the shaft. Size and location are important factors we will inspect when evaluating the quality of the concrete shaft. The flow chart of the simulation can be found in Figure 3. In the simulation, the ability of the optical-fiber-based TIP and the conventional TIP to detect defect size and location will be compared and discussed.

3. Result and Discussion

In this section, we discuss the result of simulations using two different ways to extract data based on the concept of different TIP methods. Location and size of the defects are considered. First, we compare the results from two methods regarding how defect location will affect the result. Then, we investigate how defect size will affect the result.

Table 1: Soil properties.

Properties	Unit	Value
Density	kg/m^3	1800
Soil solid thermal conductivity	W/m·K	5
Water thermal conductivity	W/m·K	0.5
Air thermal conductivity	W/m·K	0.05
Soil solid heat capacity	J/(kg·K)	850
Water heat capacity	J/(kg·K)	4190
Porosity	%	51.1
Water content	%	39.8
Saturation	%	97

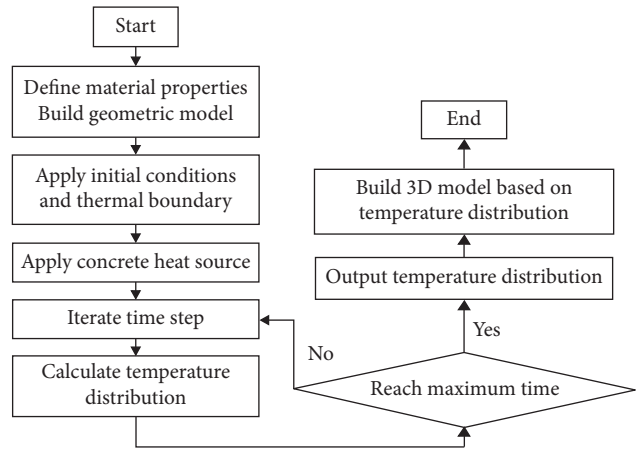

Figure 3: Flow chart.

3.1. Location Prediction. When performing TIP, we consider the location of the peak value as the location of the defect. To compare the accuracy of both methods, numerical simulation of a 6-foot diameter concrete shaft with a 12-inch sized cubic defect at selected locations is conducted. The location and size of defects are listed in Table 2. The location selected would be: defect is exactly at the measurement point of access tube method, defect is shifted from measurement point of access tube method, and defect is between measurement points of access tubes, separately (Figure 4). The result is shown in Figure 5; the concave region indicates the region that has negative value of temperature divergence. The region with dark blue color is the determination of defect by each method. The area of dark blue region indicates the size of the defect, whereas the location of that region indicates the location of the defect.

When the defect is located at the position where the infrared thermal probe measures temperature, both methods provide accurate determination of location. Furthermore, the temperature distribution can roughly indicate the shape of the defect. When the defect is shifted from the position where the infrared thermal probe measures temperature, although both methods can detect the defect, the result from conventional TIP method deviates from the actual location of the defect. At the same time, the optical-fiber-based TIP method can still have an accurate prediction of defect location. When the defect happened to be located between two measurement points of the conventional TIP method, although both methods can detect the defect, the result from

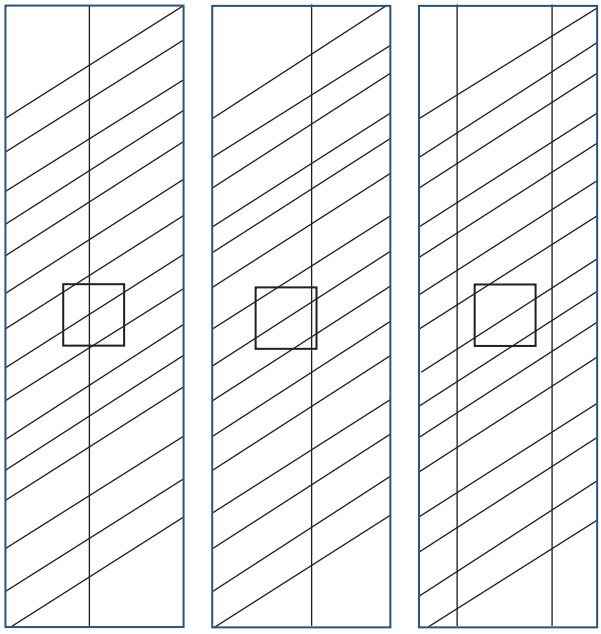

Figure 4: Schematic of defect location. (a) Defect located on access tube, (b) defect shifted from access tube, and (c) defect located between access tubes.

the conventional TIP method can hardly predict the location of the defect. The temperature distribution between access tubes does not show a significant peak value. The location of the defect can be anywhere within the low temperature region. Optical-fiber-sensor-based TIP, on the other hand, can still have an accurate determination of the defect.

According to the result presented above, in all three situations, the optical-fiber-based TIP method has great outcome despite the location of the defect. The even distribution of measurement points and relatively small interval not only increase the possibility of the defect being located at the measurement point, but also diminish the effect when the peak value is not located at the measurement point, which contributes to more accurate reconstructed temperature distribution.

Considering that in most situations, the defect is not located exactly at the measurement point, we could draw a conclusion that the optical-fiber-based TIP method would always have the same or better determination of defect location.

3.2. Size Sensitivity. The size of the defect is also a significant factor that needs to be considered for shaft integrity test. The size of defect is related to the magnitude of temperature divergence. The peak value of temperature distribution is crucial to determine the size of the defect. To compare the accuracy of both methods, numerical simulation of a 6-foot concrete shaft is conducted with different defects of different sizes located between access tubes (Table 3). The size of the defects is 18 inches, 15 inches, and 10 inches (Figure 6). An anomaly that has 12% of area reduction is an anomaly needed for further evaluation. Both methods should have the ability to detect defects at this size.

The result is shown in Figure 7; the concave region indicates that the region that has a negative value of temperature divergence. The region with dark blue color is the determined defect by each method. The area of dark blue region indicates the size of the defect, whereas the location of that region indicates the location of the defect.

When the defect is a 15-inch cube at the lateral surface of the concrete shaft, both methods can detect the existence of the defect. However, the optical fiber method has a larger temperature divergence, closer to the actual temperature distribution in that region. When the defect is a 10-inch cube at the lateral surface of concrete shaft, the infrared thermocouple probe or embedded sensor-based TIP cannot detect the defect between access tubes. The temperature divergence caused by the defect would only be maintained within a certain zone. Once the effect zone is located totally between access tubes, conventional TIP may miss the existing defect which may have a negative effect on the performance of the concrete shaft. The optical-fiber-based TIP method can still detect defects. The area of defect is smaller compared with the result shown in Figure 7, indicating that the size of the defect is smaller than the result shown in Figure 7. This demonstrates that the TIP method has the ability to measure size based on the temperature distribution result.

Since the size of defect is related to the magnitude of temperature divergence, accurate temperature distribution is crucial to defect size evaluation. The value of peak temperature divergence decreases from the center of defect outward. As distance from center of defect increase, the temperature distribution would be closer to the intact part. The closer the measurement point is to the center of the defect, the higher the accuracy of temperature distribution measurement would be. The conventional TIP has no measurement point between access tubes, which limits the minimum size of defect that can be detected. Optical-fiber-based TIP, on the other hand, has the ability to detect smaller defects due to high spatial resolution. However, if the size of the defect is too small, even optical-fiber-based TIP will not be able to detect it.

4. Conclusion

In this paper we proposed an optical-fiber-based TIP method. This method can be an improvement of infrared thermocouple probes and embedded sensors which are applied to conventional TIP by having high spatial resolution temperature data. The method also changes the way to deploy sensors from vertically deployed to spirally deployed around the reinforcement cage. These two changes enable TIP to measure a high resolution and consistent temperature distribution within the concrete shaft, leading to more accurate determination of integrity of the concrete shaft.

To verify the advantages of optical-fiber-based TIP, we investigate two factors of defects: location and size. In the location section, we set three situations: defect on access tube, shift from access tube, and between access tubes. When

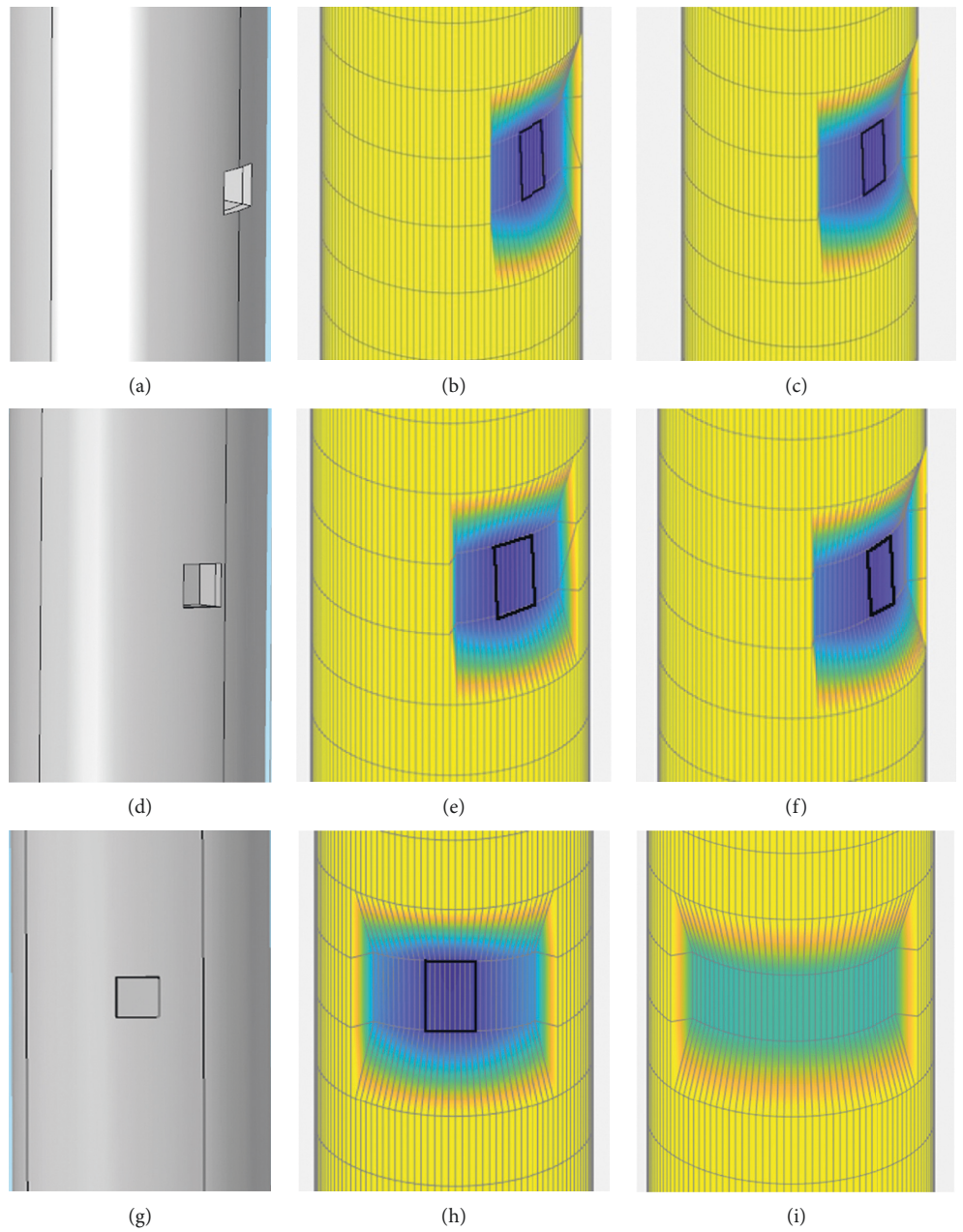

Figure 5: Result of simulation with different locations. (a, d, g) Actual location of defect, (b, e, h) location determination by the optical fiber method, and (c, f, i) location determination by the conventional method.

Table 2: Location determination by different methods.

Situation	Actual location			Optical fiber method			Conventional method		
	Depth	θ	r	Depth	θ	r	Depth	θ	r
On tube	7.5 m	180	0.6096	7.58 m	179.7	0.6148	7.58 m	181	0.6148
Around tube	7.5 m	171	0.6096	7.575 m	169	0.6175	7.575 m	179.7	0.619
Between tubes	7.5 m	150	0.6096	7.576 m	149.1	0.6096	N/A	N/A	0.774

the defect is located exactly on the access tube, both methods have an accurate determination of the location. However, when the defect is located between access tubes where conventional TIP does not have a measurement point, optical-fiber-based TIP shows higher accuracy on location determination. We also simulate three situations with different size defects located between access tubes. Since optical-fiber-based TIP has measurement points evenly

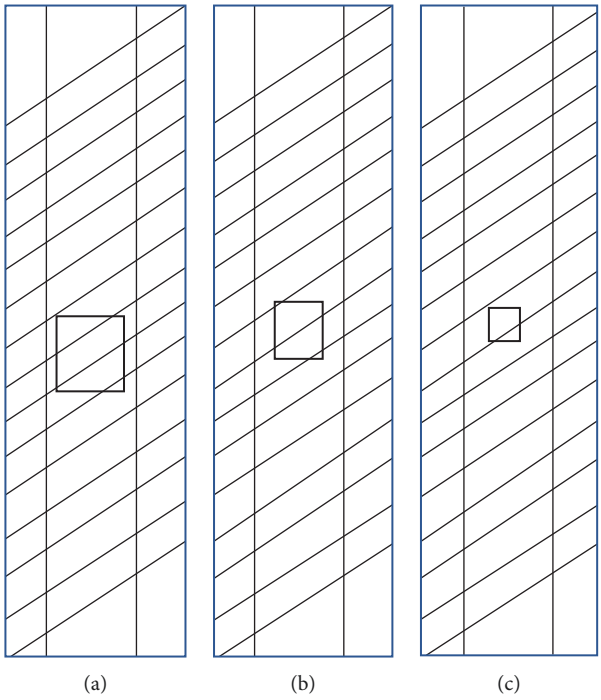

Figure 6: Schematic of defect location. (a) 18-inch cube, (b) 15-inch cube, and (c) 10-inch cube.

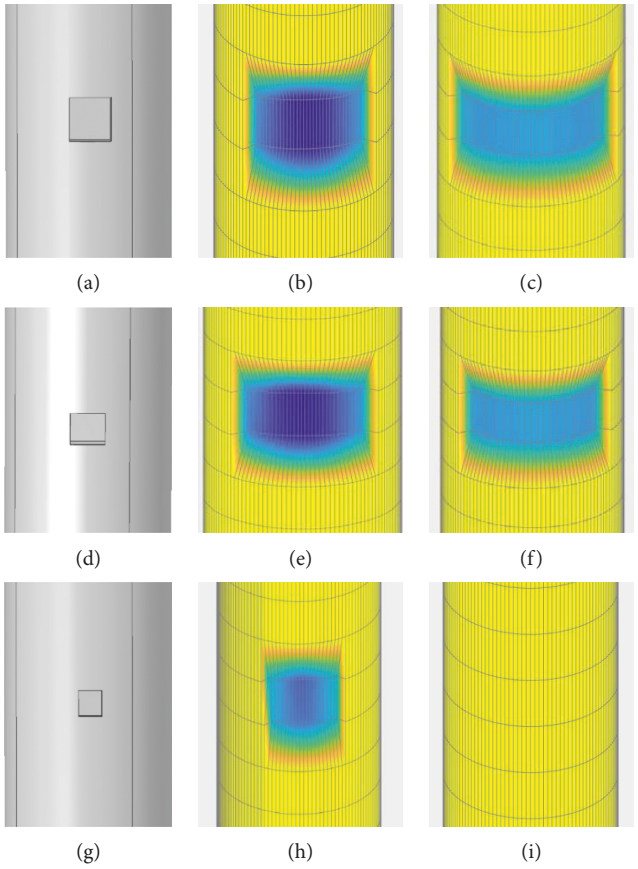

Figure 7: Result of simulation with different sizes. (a, d, g) Actual size of defect, (b, e, h) size determination by the optical fiber method, and (c, f, i) size determination by the conventional method.

Table 3: Size determination.

Actual size	Optical fiber method	Conventional method
18-inch cube	17.60 inches	13.34 inches
15-inch cube	14.68 inches	10.90 inches
10-inch cube	9.84 inches	5.45 inches

distributed at the surface, the sensitivity of optical-fiber-based TIP to the size of the defect is significantly higher. In the simulation regarding the shape of the defect, since measurement points of optical-fiber-based TIP distribute evenly within the defect, a more precise outline of the defect is depicted by optical-fiber-based TIP. Overall, optical-fiber-based TIP shows higher accuracy in prediction of shaft defects.

Data Availability

The data used to support the findings of this study are available from the corresponding author upon request.

Conflicts of Interest

The authors declare that they have no conflicts of interest.

Acknowledgments

This material is based on the work supported as part of the University of Missouri Research Board at the University of Missouri system. Additional support was provided by the Geotechnical Engineering program and Center for Advancing Faculty Excellence of Missouri University of Science and Technology. The authors would like to thank Dr. Jie Huang's valuable discussion on this problem.

References

[1] M. O'Neill, *Integrity Testing of Foundations*, Transportation Research Board, Washington, DC, USA, 1991.

[2] O. Klingmuller and F. Kirsch, *Current Practices and Future Trends in Deep Foundations*, American Society of Civil Engineers, Reston, VA, USA, 2004.

[3] D. Brown and A. Schindler, "High performance concrete and drilled shaft construction," in *Proceedings of GSP 158 Contemporary Issues in Deep Foundations*, Denver, CO, USA, February 2007.

[4] N. Massoudi and W. Teffera, "Non-destructive testing of piles using the low strain integrity method," in *Proceedings of 5th International Conference on Case Histories in Geotechnical Engineering*, pp. 13–17, Missouri University of Science and Technology, New York, NY, USA, April 2004.

[5] J. C. Ashlock and M. K. Fotouhi, "Thermal integrity profiling and crosshole sonic logging of drilled shafts with artificial defects," in *Proceedings of Geo-Congress 2014 Technical Papers, GSP 234 © ASCE*, Atlanta, Georgia, February 2014.

[6] S.-J. Hsieh, R. Crane, and S. Sathish, "Understanding and predicting electronic vibration stress using ultrasound excitation, thermal profiling, and neural network modeling," *Nondestructive Testing and Evaluation*, vol. 20, no. 2, pp. 89–102, 2005.

[7] D. Li, L. Zhang, and W. Tang, "Closure to "reliability evaluation of cross-hole sonic logging for bored pile integrity" by

D. Q. Li, L. M. Zhang, and W. H. Tang," *Journal of Geotechnical and Geoenvironmental Engineering*, vol. 133, no. 3, pp. 343-344, 2007.

[8] K. Johnson, G. Mullins, and D. Winters, "Concrete temperature control via voiding drilled shafts," in *Proceedings of Contemporary Issues in Deep Foundations, ASCE Geo Institute, GSP 158*, no. 1, pp. 1–121, Denver, CO, USA, October 2007.

[9] K. R. Johnson, "Temperature prediction modeling and thermal integrity profiling of drilled shafts," in *Proceedings of Geo-Congress 2014 Technical Papers, GSP 234 © ASCE*, Atlanta, Georgia, February 2014.

[10] G. Mullins, "Thermal integrity profiling of drilled shafts," *DFI Journal-The Journal of the Deep Foundations Institute*, vol. 4, no. 2, pp. 54–64, 2010.

[11] G. Mullins, "Advancements in drilled shaft construction, design, and quality assurance: the value of research," *International Journal of Pavement Research and Technology*, vol. 6, no. 2, pp. 993–999, 2013.

[12] K. R. Johnson, "Analyzing thermal integrity profiling data for drilled shaft evaluation," *DFI Journal-The Journal of the Deep Foundations Institute*, vol. 10, no. 1, pp. 25–33, 2016.

[13] A. G. Davis, "Assessing reliability of drilled shaft integrity testing," *Transportation Research Record*, vol. 1633, pp. 108–116, 1998.

[14] D. Samiec, *Distributed Fiber Optic Temperature and Strain Measurement with Extremely High Spatial Resolution*, Polytech GmbH, Waldbronn, Germany, 2011.

[15] W. Pei, W. Yua, S. Li, and J. Zhou, "A new method to model the thermal conductivity of soil–rock media in cold regions: an example from permafrost regions tunnel," *Cold Regions Science and Technology*, vol. 95, pp. 11–18, 2013.

[16] T. J. Moore, M. R. Jones, D. R. Tree, and D. D. Allred, "An inexpensive high-temperature optical fiber thermometer," *Journal of Quantitative Spectroscopy and Radiative Transfer*, vol. 187, pp. 358–363, 2017.

[17] H. Su, H. Jiang, and M. Yang, "Dam seepage monitoring based on distributed optical fiber temperature system," *IEEE Sensors Journal*, vol. 15, no. 1, pp. 9–13, 2015.

[18] R. K. Palmer, K. M. McCary, and T. E. Blue, "An analytical model for the time constants of optical fiber temperature sensing," *IEEE Sensors Journal*, vol. 17, no. 17, pp. 5492–5511, 2017.

[19] A. Leal-Junior, A. Frizera-Neto, C. Marques, and M. Pontes, "A polymer optical fiber temperature sensor based on material features," *Sensors*, vol. 18, no. 2, p. 301, 2018.

[20] Y. Rui, C. Kechavarzi, O'. L. Frank, C. Barker, D. Nicholson, and K. Soga, "Integrity testing of pile cover using distributed fibre optic sensing," *Sensors*, vol. 17, no. 12, p. 2949, 2017.

[21] Y. Cardona-Maya and J. F. Botero-Cadavid, "Refractive index desensitized optical fiber temperature sensor," *Revista Facultad de Ingeniería*, no. 85, pp. 86–90, 2017.

[22] J. Huang, X. Lan, M. Luo, and H. Xiao, "Spatially continuous distributed fiber optic sensing using optical carrier based microwave interferometry," *Optics Express*, vol. 22, no. 15, pp. 18757–18769, 2014.

[23] A. Schindler and K. Folliard, "Heat of hydration models for cementitious materials," *ACI Materials Journal*, vol. 102, no. 1, pp. 24–33, 2005.

[24] W. Liu, P. He, and Z. Zhang, "A calculation method of thermal conductivity of soils," *Journal of Glaciology and Geocryology*, vol. 24, no. 6, pp. 770–773, 2002.

[25] C. S. Blázquez, A. F. Martín, I. M. Nieto, and D. Gonzalez-Aguilera, "Measuring of thermal conductivities of soils and rocks to be used in the calculation of a geothermal installation," *Energies*, vol. 10, no. 795, pp. 1–19, 2017.

[26] D. Barry-Macaulay, A. Bouazza, R. M. Singh, B. Wang, and P. G. Ranjith, "Thermal conductivity of soils and rocks from the Melbourne (Australia) region," *Engineering Geology*, vol. 164, pp. 131–138, 2013.